We are IntechOpen, the world's leading publisher of Open Access books Built by scientists, for scientists

4,800
Open access books available

122,000
International authors and editors

135M
Downloads

Our authors are among the

154
Countries delivered to

TOP 1%
most cited scientists

12.2%
Contributors from top 500 universities

CLARIVATE ANALYTICS BOOK CITATION INDEX INDEXED

WEB OF SCIENCE™

Selection of our books indexed in the Book Citation Index in Web of Science™ Core Collection (BKCI)

Interested in publishing with us?
Contact book.department@intechopen.com

Numbers displayed above are based on latest data collected.
For more information visit www.intechopen.com

11

Electron transport effect on optical response of quantum-cascade structures

Mykhailo Klymenko and Oleksiy Shulika
Kharkov National University of Radio Electronics
Ukraine

Igor Sukhoivanov
University of Guanajuato
Mexico

1. Introduction

The quantum-cascade laser is an unique source of the THz laser radiation operated in continuous-wave and pulse regimes [Gmachl et al (2001)]. History of these lasers counts more than ten years. However, many aspects of the carrier transport and interaction with light field are still unclear. Very important question concerning physics of the quantum-cascade structures (QCS) is the following: which kind of transport, coherent or incoherent, is prevailed in QCS? There were many discussions about the problem, and several attempts to estimate kind of transport were successful especially [Iotti et al (2001)],[Weber et al (2009)]. The answer on this question depends on conditions of QCS operation. For example, the coherent electron transport is of interest in the non-equilibrium regime at femtosecond and picosecond time intervals. The incoherent transport is prevalent at the high excitation level in the stationary quasi-equilibrium regime. In both cases, the electron transport influence on optical properties of the device. In this connection, the development of the theory for coherent and incoherent electron transport regimes, included many-body effects and light-matter interactions in QCS, is of actual interest.

In this chapter, we provide modeling of optical and transport properties of QCS uncovering influence of the electron transport on optical characteristics. Lasing, light absorption and spontaneous emission in QCS are accompanied and affected by many complicated transport processes such as electron diffusion, drift, tunneling, recombination, generation, capture and escape mediated by electron-electron, electron-phonon and electron-photon scattering events [Piprek (2005)]. Most of these effects can be treated within the quasi-equilibrium approximation. However, the approximation is not valid at ultrashort time intervals which are of interest nowadays due to rapid development of the femtosecond spectroscopy for semiconductor nanostructures [Rulliere (2005)]. Other area demanding consideration of ultra-fast non-equilibrium processes is THz emitting of QCS in the pulse regime; that is under rapid development currently due to promising applications in fundamental and applied science [Lee (2009)].

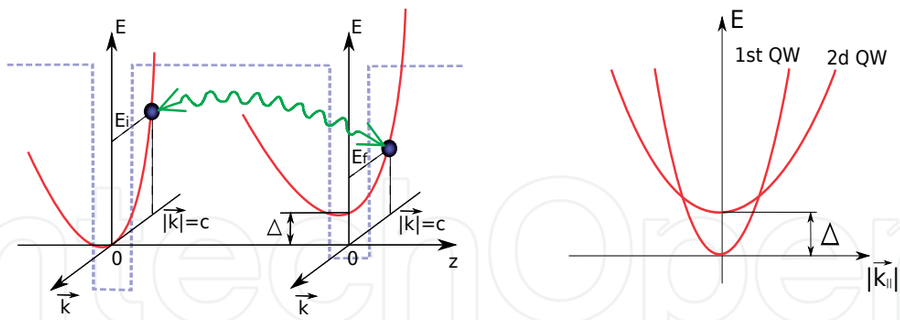

Fig. 1. Coherent electron transport between two quantum wells with subband structure via tunneling

To predict output optical characteristics of the quantum-cascade lasers, it is necessary to simulate dynamics of electrons, holes and photons in the non-equilibrium state. The peculiarity of QCS is that the system is related to the open quantum systems. Moreover, the structure is characterized by pronounced non-equilibrium regime of operation. There are several approaches to modelling the transport in such a system. One of them is based on non-equilibrium Green's functions [Lee et al (2002)], another one is based on the density matrix theory [Iotti et al (2001)]. These two are not the only approaches to modeling transport in QCS. For example, rate equations are widely used in connection to this problem [Vukmirović (2005)]. However, these two methods are most rigorous and controllable. They can be realized at various levels of approximation and allow to estimate approximation error. In ideal case, they do not require any fitting parameter and give results *ab initio*. Our consideration in this chapter is based on the density matrix theory. As a result, we will derive kinetic equations describing dynamics of carriers, polarization and inter-quantum-well tunneling currents for non-equilibrium regime of the operation, and then, we discuss main features of transport and optical properties of QCS.

2. Coherent and incoherent transport

2.1 Coherent transport

In this section, we will represent theoretical instruments proper for high accuracy modeling of the electron transport in QCS. Up to date, many efforts have been made and much progress has been achieved in modeling of the electron transport in QCS. Especially, it concerns stationary operating regime. Recently, advance in modeling of femtosecond optical response of QCS has been reached [Iotti et al (2001)], [Weber et al (2009)]. Most successful approaches to electron transport modeling have been realized applying the density matrix theory [Meier (2007)]. This theory is especially suitable for the large open quantum systems with many-body interactions. Therefore, we apply exactly the density matrix theory to realize systematic treatment of the coherent and incoherent electron transport in semiconductor nanostructures.
Here, the simplest model heterostructure consisting of two interacting quantum wells is considered to make statements compact and clear. The sketch of energy levels for such a structures is shown in Fig. 1.

Electron states in each quantum well are characterized by single-band structure when quantum wells are uncoupled. The band structure, shown in Fig. 1(b), can be analytically expressed as:

$$\varepsilon_{1,k} = E_1 + \frac{\hbar^2 k^2}{2m_1}, \tag{1}$$

$$\varepsilon_{2,k} = E_2 + \frac{\hbar^2 k^2}{2m_2} = E_1 + \Delta + \frac{\hbar^2 k^2}{2m_2}. \tag{2}$$

The electron in each quantum well is characterized by continuous energy spectra and has states $|1,k\rangle$ in one quantum well and $|2,k\rangle$ in another one. The number in the ket vector corresponds to the subband kind and the letter is the in-plane electron wave vector limited by the 1st Brillouin zone (axial approximation is applied [Haug (2004)]). States should satisfy completeness conditions [Meier (2007)]:

$$\hat{1} = \sum_j \sum_k |j,k\rangle\langle k,j|. \tag{3}$$

In practice, each quantum well and barrier layer can be made of different semiconductor materials. This means that each quantum well can be characterized by own width, depth and effective masses. That is why, we consider subband dispersion curves which are shifted relative each other by some value Δ and characterized by different curvature.
It is well known that, if one turns on the interaction between quantum wells, the quantum states of whole system are changed and each state of the system is splitted into bound and antibound state. That is the picture for the stationary regime. However, the case of interest is the time evolution of the system that is prepared in some non-stationary state in the initial time moment. Even though quantum system is prepared in some defined stationary state, following artificial modification of the system (by measurement event for example) can change the energy spectrum and the ininial state is not stationary anymore. This leads to nontrivial dynamical evolution of observables. Considered here open quantum systems are interacted with environment that leads to modifications of its parameters and dynamical evolution of observables. Therefore, we focus on the case when the sysatem is prepared in the stationary state of noninteracted quantum wells with following turning on of interactions.
The Hamiltonian for considered model system can be represented in the form:

$$\hat{H} = \hat{H}_1 + \hat{H}_2 + \hat{H}_{int}, \tag{4}$$

here: $\hat{H}_1$ is Hamiltonian for the first quantum well, $\hat{H}_2$ is Hamiltonian for the second quantum well and $\hat{H}_{int}$ describes the interaction between quantum wells.

Acting by the unity operator from left and right sides on the Hamiltonian, one gets:

$$\hat{H} = \hat{1} \cdot \hat{H} \cdot \hat{1} = \sum_k \left(\varepsilon_{1,k}|1,k\rangle\langle k,1| + \varepsilon_{2,k}|2,k\rangle\langle k,2|\right) + \sum_{i \neq j} \sum_k h_{ij}|i,k\rangle\langle k,j|, \tag{5}$$

where: h_{ij} is the coupling coefficient describing the intensity of interactions between quantum wells.

As far as considered structure is the open quantum system, we use trusted instrument from the quantum statistical physics that is the density operator:

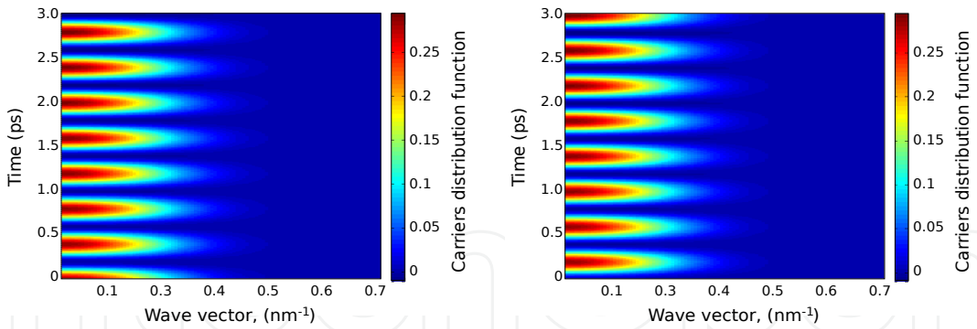

Fig. 2. Time-dependent electron distribution function for a) the left quantum well and b) right quantum well having the same band structure

$$\hat{\rho} = |t\rangle\langle t|. \tag{6}$$

The density operator can be represented in the matrix form using defined system of basis functions. As an example, we build matrix representation of the density operator using basis $|j,k\rangle$ defined above:

$$\rho_k = \langle k,i|\hat{\rho}|j,k\rangle = \begin{pmatrix} \rho_{11} & \rho_{12} \\ \rho_{21} & \rho_{22} \end{pmatrix} = \begin{pmatrix} |\langle k,1|t\rangle|^2 & \langle k,1|t\rangle\langle t|2,k\rangle \\ \langle k,2|t\rangle\langle t|1,k\rangle & |\langle k,2|t\rangle|^2 \end{pmatrix}. \tag{7}$$

Diagonal elements describe the probability of finding the electron at the time t in some defined energy band. Nondiagonal elements corresponds to some kind of correlations which give probability of the particle transition between states at the time t. The non-diagonal matrix elements are related to microscopic polarization or currents. In turn, the polarization is directly related to the electrical current according to classical electrodynamics as well as quantum one.

Time evolution of the density operator is defined by the Liouville-von Neumann equation [Meier (2007)]:

$$i\hbar\frac{\partial\rho}{\partial t} = [H,\hat{\rho}]_+. \tag{8}$$

In the Heisenberg representation, this equation is coincided with the Heisenberg equation for time-dependent operators. Eq. 8 can be written related to each element of the density matrix using quantum-mechanical averaging with the basis defined above . Resulting system of equations reads:

$$i\hbar\frac{\partial\rho_{11,k}}{\partial t} = h_{12,k}\left(\rho_{21,k} - \rho_{12,k}\right), \tag{9}$$

$$i\hbar\frac{\partial\rho_{22,k}}{\partial t} = -h_{12,k}\left(\rho_{21,k} - \rho_{12,k}\right), \tag{10}$$

$$i\hbar\frac{\partial\rho_{12,k}}{\partial t} = \left(\varepsilon_{2,k} - \varepsilon_{1,k}\right)\rho_{21,k} + h_{12,k}.\left(\rho_{22,k} - \rho_{11,k}\right) \tag{11}$$

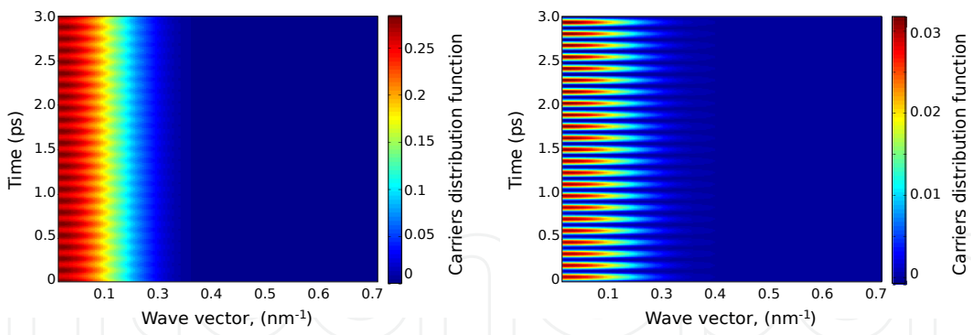

(a) (b)

Fig. 3. Time-dependent electron distribution function for a) the left quantum well and b) right quantum well having bands shifted on 30 meV relative to each other

These are ordinary differential equations also known as kinetic equations. The number of equations is equal $3N_k$, where N_k is the number of discretization points in k-space. Eqs. (9)-(11) are written for some defined point k in the Brillouin zone. To analyze electron transport in our simple model system, we should solve this system of equations analytically or numerically. Here, we choose the second way to show general approach to such a mathematical problem. The fourth order Runge-Kutta method is applied to solve the problem. This method is stable and accurate enough to satisfy our requirements on CPU time and computational accuracy. As far as we deal with first order ordinary differential equations, the initial condition should be added. We assume that, at the initial time, all electrons are located in the 1st noninteracting quantum well with some defined distribution function. Initial distribution is chosen to be the Fermi-Dirac distribution with some defined temperature and Fermi level ($T = 300$ K and $E_f = \varepsilon_{1,0}$). Solutions of kinetic equations are time dependencies of microcurrents or polarizations and electron distribution functions for each band and each value of the in-plane wave vector k. At the initial time, interaction between quantum wells is turning on that is reflected in the coupling coefficient:

$$h_{12,k} = \begin{cases} 0, & t < 0; \\ const, & t \geq 0. \end{cases} \tag{12}$$

Let us consider first the effect of band structure on electron transport. Solving of the equations for two identical subbands, one obtains the result shown in Fig.2. Electrons oscillate between quantum wells through the barrier. The frequency of oscillations is determined only by the coupling coefficient. At some instant times, all electrons totaly depopulate the band in a quantum well transiting to another one.

In the case, when bands have the same shape and are shifted relative to each other, the electron distribution function is characterized by the time dependence shown in Fig. 3. The mismatch of energy levels leads to decreasing of electrons amount passing through the barrier. Most of particles do not leave the state occupied at the initial time moment. In particular case represented in Fig. 3, band mismatch is equal 30 meV and the maximal fraction of passed particles amounts 10 %.

Also, changes of the oscillation frequency is observed. Thus, the frequency of oscillations is dependent on the band mismatch as well as coupling coefficient. Explicit dependence could be

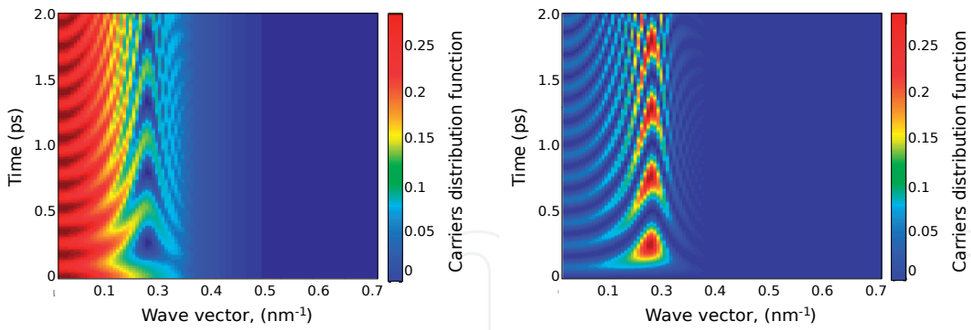

(a) (b)

Fig. 4. Time-dependent electron distribution function for a) the left quantum well and b) right quantum well having bands with different effective masses

derived from equations (9)-(11). This can be realized by Fourier transformation of equations with following algebraic manipulations. The result reads:

$$\omega = \frac{1}{2\hbar}\sqrt{\Delta^2 + 4h_{12,k}}, \tag{13}$$

here Δ is the band mismatch shown in Fig.1.

Another approach to obtaining this result is solving of the stationary Schrödinger equation for coupled quantum wells. The oscillation frequency is proportional to splitting of energy levels caused by resonant tunneling [Meier (2007)].
As far as each quantum well can be characterized by own width, depth and effective masses, we will provide investigation of the coherent electron transport between bands with different curvature of dispersion dependencies. As an example, let us consider two bands shown in Fig. 1(b) having parameters $E_1 = 0.03$, $E_2 = 0$, $m_1 = 5m$ and $m_2 = m$.
Band dispersion curves are crossed at the point $k = 0.27nm^{-1}$. The most part of electrons are propagated with this non-zero in-plane wave vector and oscillation frequency is dependent on the electron in-plane wave vector (see Fig. 4(b)). The lowest frequency corresponds to minimal gap between bands. That is in agreement with formula (13).

2.2 Incoherent transport

All cases of electron transport considered above are related to the coherent electron transport due to any decoherence effect has not been included in the consideration yet. Decoherence can be caused by scattering events leading to relaxation into the stationary equilibrium state. Thus, one should include additional term in the Hamiltonian (4) describing scatterings.

$$\hat{H} = \hat{H}_1 + \hat{H}_2 + \hat{H}_{int} + \hat{H}_{scatt}. \tag{14}$$

It is necessary to note that the single-particle formalism used above is not applicable directly to scattering processes, because such processes are essentially many-body effects. However, some approximation can conserve the problem be single-particle. For example, one can apply the mean-field approximation to the many-body problem. This approach is often used in

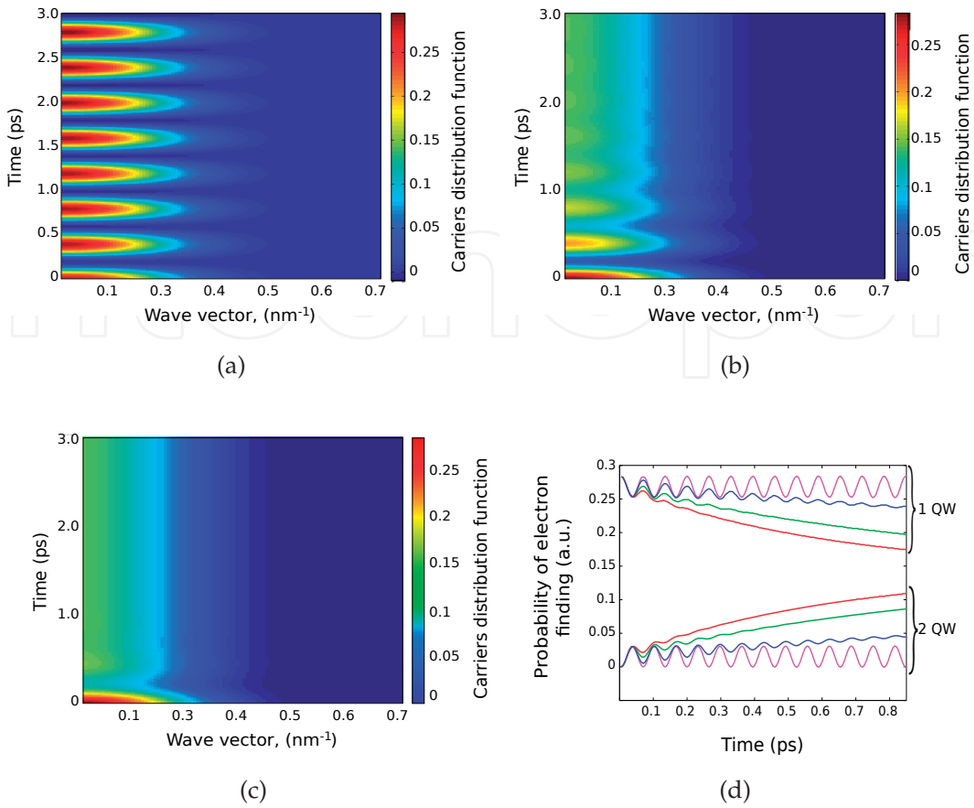

Fig. 5. Time evolution of the electron distribution function for a) $\gamma = 10ps$, b) $\gamma = 1.5ps$ and c) $\gamma = 0.5ps$ and d) $k = 0$, band mismatch $\Delta = 0.03eV$ and dephasing times taken from the previous case.

connection with phenomenological relaxation and dephasing times describing influence of many-body effects on single-particle equations.
Formally, effect of the scattering term in (14) can be represented in Eqs. (9)-(11) by additional terms at the right side of kinetic equations.

$$i\hbar\frac{\partial\rho_{11}}{\partial t} = h_{12}\left(\rho_{21}-\rho_{12}\right) + \left.\frac{\partial\rho_{11}}{\partial t}\right|_{scatt}, \tag{15}$$

$$i\hbar\frac{\partial\rho_{22}}{\partial t} = -h_{12}\left(\rho_{21}-\rho_{12}\right) + \left.\frac{\partial\rho_{22}}{\partial t}\right|_{scatt}, \tag{16}$$

$$i\hbar\frac{\partial\rho_{12}}{\partial t} = \left(\varepsilon_2-\varepsilon_1\right)\rho_{21} + h_{12}\left(\rho_{22}-\rho_{11}\right) + \left.\frac{\partial\rho_{12}}{\partial t}\right|_{scatt}, \tag{17}$$

These additional terms can be computed *ab initio* using many-body theory and a set of approximations which will be represented in the next section. Here, we use phenomenological relaxation and dephasing times to investigate many-body effects. In this case, Eqs. (15)-(17) are modified as follows:

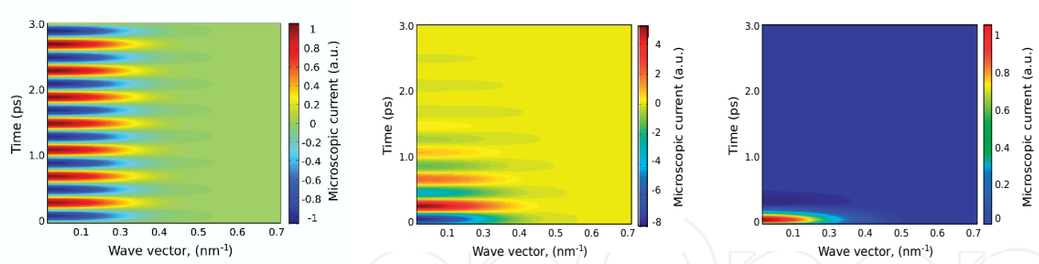

(a) (b) (c)

Fig. 6. Microscopic currents for a) $\gamma = 10ps$, b) $\gamma = 1.5ps$ and c) $\gamma = 0.5ps$

$$i\hbar\frac{\partial\rho_{11}}{\partial t} = h_{12}\left(\rho_{21} - \rho_{12}\right) - \frac{i(\rho_{11} - f_1)}{\tau}, \tag{18}$$

$$i\hbar\frac{\partial\rho_{22}}{\partial t} = -h_{12}\left(\rho_{21} - \rho_{12}\right) - \frac{i(\rho_{22} - f_2)}{\tau}, \tag{19}$$

$$i\hbar\frac{\partial\rho_{12}}{\partial t} = \left(\varepsilon_2 - \varepsilon_1\right)\rho_{21} + h_{12}\left(\rho_{22} - \rho_{11}\right) - \frac{i\rho_{12}}{\gamma}. \tag{20}$$

here γ is the dephasing time, τ is the relaxation time, f_1 and f_2 are stacionary electron distributions in each quantum well.

Relaxation and dephasing times can be determined from experimental data (optical pump-probe experiments [Vu (2006)]). If the total number of electrons is time-independent, the relaxation times tend to infinity and the last terms in Eq.(18) and (19) can be neglected. This is the case considered in this section. Thus, we will investigate the effect of dephasing only. Time dependencies of electron distribution function are shown in Fig. 5 for different dephasing times. Corresponding microscopic currents are shown in Fig. 6.
Microscopic currents reflects the probability of electron transition from one quantum well to another. Dephasing leads to decay of oscillations and becoming of the stationary distribution of electrons. If dephasing is absent (dephasing time is very high), the electron transport is pure coherent (see Fig. 5(a)). In Fig. 5(c), another limit case is shown when the dephasing time is very small. In this case, the transient process require few time and stationary regime becomes very fast. The transient process occurs because the quantum system is prepared in non-stationary state at the initial time, and it tends to the stationary state. Scattering events allow energy quanta exchange between particles leading to the relaxation into the stationary state. As follows from Fig. 6(c), particle exchange between quantum wells occurs at short time interval when the dephasing time is great.
The evolution of the electron distribution function for zero in-plane wave vector (k=0) is shown in Fig. 5(d) for the case when bands are shifted relative each other by 30 meV. In this case, dephasing times are the same as in previous examples. Dephasing leads to leveling of electron concentration in each quantum well and becoming of the stationary state. Oscillations of the electron distribution function are decayed with increasing of the dephasing time. The result of dephasing absence is endless oscillations of the electron distribution function and asymmetrical population of subbands.

3. Optical response

3.1 Model structure and its Hamiltonian

As we did in the previous section, we introduce here the new model structure that reflects main effect in the QCS and is still simple enough for modeling and analysis. Effects of interest are light-matter interactions together with transport processes in the structure.

In this section, we focus our attention on optical processes in the QCS with vertical transitions [Faist (1995)]. Term "vertical transitions" means that photon assisted tunneling is excluded from the consideration. The QCS have N optical-sensitive active regions which interact with each other via exchanging of electrons through injectors. The Hamiltonian of the system reads:

$$H = \sum_{j=1}^{N} H_j + \sum_{j=1}^{N-1} H_{j,j+1} + H_L + H_R + H_{L,1} + H_{N,R}. \tag{21}$$

The first sum in RS contains electron kinetic energy, electron scattering and light-matter interaction terms for all active regions. The second sum describes electron transport through injectors. The term H_L and H_R corresponds to the energy of regions terminated considered planar structure at the both sides. Finally, terms $H_{L,1}$ and $H_{N,R}$ describe exchanging of electrons between the structure and terminal regions. Such expression of Hamiltonian is quite natural if all optical transitions appear inside active regions. This is our case because the QCS with vertical transitions is under consideration [Faist (1995)]. The terminal regions shown in Fig. 7(c) as circles is implemented artificially. These regions include the whole rest space of the system except some considered region been of interest. Necessity of such regions is caused by influence of environment in the open quantum system. Modeling of all periods of QCSs requires much computational resources. So, the second reason of terminal regions application is the approximation allowing to consider dynamical behavior of electrons only in one or several periods. In this case, whole rest structure is assumed to be in the quasi-equilibrium state, and it is contained in the terminal regions. We use approximation that the terminal regions are characterized by some kind of stationary distribution function. We call them bathes in analogy to statistical mechanics. Alternative approach is application of periodic boundary conditions [Lee et al (2002)].

In this section, we consider only one period of the QCS. Corresponding model structure is shown in Fig. 7(c). It contains only one active region surrounded by two injectors and two terminal regions. The Hamiltonian for the model structure consist of five terms in the simplest case, when many-body effects are not considered:

$$H = H_L + H_R + H_a + H_{La} + H_{aR}, \tag{22}$$

where H_L is the energy of the left reservoir, H_R is the energy of the right reservoir, H_a is the energy of the active region, H_{La} and H_{aR} describe transitions between reservoirs and the active region.

In the active regions, light-matter interactions proceed involving electron-phonon, electron-electron and electron-impurity scatterings. Thus, we should include into consideration many-body effects to simulate the optical response of the semiconductor media correctly. The approximations that all many-body effects appear in the active region is applied. In this case, the Hamiltonian for the active region reads:

$$H_a = H_{kin} + H_I + H_{ph-el} + H_{el-el} + H_{el-imp}, \tag{23}$$

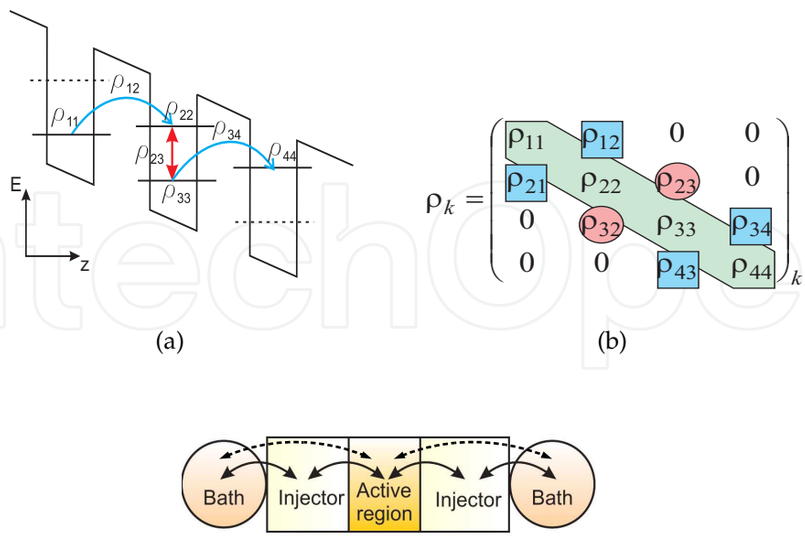

Fig. 7. Electron transitions (a), density matrix (b) and configuration (c) for the model structure

where: H_{kin} is the kinetic energy term; H_I is the light-matter interactions term; H_{ph-el} is the photonelectron scatterings term; H_{el-el} is the electron-electron interactions term; H_{el-imp} is the electron impurities scatterings term.

In this chapter, we consider electron-electron interactions at the Hartree-Fock level of approximations. All other interactions are taken into account phenomenologically via the dephasing time. In the frame of many body theory, each term in (22) and (23) is represented as a product of field operators. They could be expanded in some set of single-particle basis functions. Expansion coefficients are creation/annihilation operators. Thus, if the basis is known, the problem can be formulated in terms of creation/anihilation operators:

$$H_{kin} = \sum_{i,k} \varepsilon_{i,k} a^{\dagger}_{i,k} a_{i,k} \quad , \tag{24}$$

$$H_L = \sum_{\kappa_1} \varepsilon_{\kappa_1} L^{\dagger}_{\kappa_1} L_{\kappa_1} \quad , \tag{25}$$

$$H_R = \sum_{\kappa_2} \varepsilon_{\kappa_2} R^{\dagger}_{\kappa_2} R_{\kappa_2} \quad , \tag{26}$$

$$H_{La} = \sum_{i,k,\kappa_1} \left(h_{i,k,\kappa_1} L^{\dagger}_{\kappa_1} a_{i,k} + h_{\kappa_1,i,k} a^{\dagger}_{i,k} L_{\kappa_1} \right) , \tag{27}$$

$$H_{aR} = \sum_{i,k,\kappa_2} \left(h_{i,k,\kappa_2} R^{\dagger}_{\kappa_2} a_{i,k} + h_{\kappa_2,i,k} a^{\dagger}_{i,k} R_{\kappa_2} \right) , \tag{28}$$

$$H_I = \sum_{k} \left(d_{12} a^{\dagger}_{1,k} a_{2,k} + d^{*}_{21} a^{\dagger}_{2,k} a_{1,k} \right) , \tag{29}$$

$$H_{el-el} = \sum_{\substack{i,j,i',j',\\ k,k',q\neq 0}} V_q^{i,j,i',j'} a^{\dagger}_{j',k'+q} a^{\dagger}_{i',k-q} a_{i,k} a_{j,k'}. \tag{30}$$

here:

$a^{\dagger}_{i,k}$	is the creation operator for the in-plane wave vector k and subband i in the active region
$a_{i,k}$	is the annihilation operator for the in-plane wave vector k and subband i in the active region
$L^{\dagger}_{\kappa_1}$	is the creation operator for the in-plane wave vector $\kappa 1$ in the left bath
L_{κ_1}	is the annihilation operator for the in-plane wave vector $\kappa 1$ in the left bath
$R^{\dagger}_{\kappa_2}$	is the creation operator for the in-plane wave vector $\kappa 2$ in the right bath
R_{κ_2}	is the annihilation operator for the in-plane wave vector $\kappa 2$ in the right bath
d_{12}	is the dipole matrix element
h_{i,k,κ_1}	is the coupling coefficient between the active region and left bath
h_{i,k,κ_2}	is the coupling coefficient between the active region and right bath
$V_q^{i,j,i',j'}$	is the Coulomb potential
k	is the in-plane wave vector for the active region
κ_1	is the in-plane wave vector for the left bath
κ_2	is the in-plane wave vector for the right bath
q	is the wave vector $q = \lvert k - k' \rvert$
i, j, i', j'	are subband indexes for the active region, $i, j, i', j' = 1, 2$

In the active region, we assume presence of only two subbands while bathes are characterized by single bands. Therefore, states in the active region have the quantum number, additional to wave vector, which is subband index $i = 1, 2$. Coupling coefficients defines properties of the transition regions between the active region and bathes. Such a transition region can be single injection barrier separating the active region and injector. Also, the whole injector can be considered as an effective barrier. The width for such a barrier is dependent on the energy and momentum of propagated particles. This approximation can be applied if electrons propagate through the injector in the ballistic transport regime (without inelastic scattering). The transmission dependence on the electron energy and momentum have been computed in [Klymenko et al (2008)] for layered structures in the ballistic limit.
The density matrix elements can be represented using creation and annihilation operators:

$$\rho_{ij,k} = \langle a^{\dagger}_{i,k} a_{j,k} \rangle. \tag{31}$$

The structure of the density matrix is represented in Fig. 7(a) and 7(b). Matrix elements at the main diagonal are probabilities of electron finding at some defined state. In other words, these elements are electron distribution functions for subbands in the active region and bathes. Elements at upper and lower subdiagonals describe transitions between subbands. The density matrix has tridiagonal structure due to the chain configuration of the transitions. It means that electron can not transit from one bath to another one avoiding the active region. That is undoubtedly an approximation and the probability of such an even exists. However, the approximation is good enough that is proved by computations of probabilities for these transitions. Squares in Fig. 7(b) indicate density matrix elements corresponding to the transitions between the active region and bathes. Circles correspond to transitions between subbands

within the active region. Hereafter, non-zero density matrix elements are expressed in terms of creation/anihilation operators:

$$P_k = \langle a^{\dagger}_{2,k} a_{1,k} \rangle, \tag{32}$$

$$n_{i,k} = \langle a^{\dagger}_{i,k} a_{i,k} \rangle, \tag{33}$$

$$n^L_{\kappa 1} = \langle L^{\dagger}_{\kappa 1} L_{\kappa 1} \rangle, \tag{34}$$

$$n^R_{\kappa 2} = \langle R^{\dagger}_{\kappa 2} R_{\kappa 2} \rangle, \tag{35}$$

$$J_{\kappa 1,i,k} = \langle L^{\dagger}_{\kappa 1} a_{i,k} \rangle, \tag{36}$$

$$J_{\kappa 2,i,k} = \langle R^{\dagger}_{\kappa 2} a_{i,k} \rangle. \tag{37}$$

In consecutive order, these are the microscopic polarization, electron distribution function in the active region, electron distribution function in the left and right bath respectively, and microscopic polarizations caused by currents from the left bath to the active region and from the active region to the right bath.
To obtain information about the time evolution of any operator product or density matrix element, one should write and then solve the system of Heisenberg equations.

$$-i\hbar \frac{P_k}{dt} = \langle \left[H, a^{\dagger}_{2,k} a_{1,k} \right] \rangle, \tag{38}$$

$$-i\hbar \frac{dn_{i,k}}{dt} = \langle \left[H, a^{\dagger}_{i,k} a_{i,k} \right] \rangle, \tag{39}$$

$$-i\hbar \frac{n^L_{\kappa 1}}{dt} = \langle \left[H, L^{\dagger}_{\kappa 1} L_{\kappa 1} \right] \rangle, \tag{40}$$

$$-i\hbar \frac{n^R_{\kappa 1}}{dt} = \langle \left[H, R^{\dagger}_{\kappa 1} R_{\kappa 1} \right] \rangle, \tag{41}$$

$$-i\hbar \frac{J_{\kappa 1,i,k}}{dt} = \langle \left[H, L^{\dagger}_{\kappa 1} a_{i,k} \right] \rangle, \tag{42}$$

$$-i\hbar \frac{J_{\kappa 2,i,k}}{dt} = \langle \left[H, R^{\dagger}_{\kappa 2} a_{i,k} \right] \rangle. \tag{43}$$

3.2 Kinetic equations

After evolution of commutators in (38)-(43), one gets following equations:

$$\frac{\partial P_k}{\partial t} = -i \left(e_{2,k} - e_{1,k} \right) P_k - i \left(n_{2,k} - n_{1,k} \right) \omega_{R,k} + \left. \frac{\partial P_k}{\partial t} \right|_{scatt}, \tag{44}$$

$$\frac{\partial n_{2,k}}{\partial t} = -2Im \left(\omega_{R,k} P^*_k \right) + 2Im \left(h_{i,k,\kappa 1} J_{\kappa 1,i,k} \right) + \left. \frac{\partial n_{2,k}}{\partial t} \right|_{scatt}, \tag{45}$$

$$\frac{\partial n_{1,k}}{\partial t} = -2Im \left(\omega_{R,k} P_k \right) + 2Im \left(h_{i,k,\kappa 2} J_{\kappa 2,i,k} \right) + \left. \frac{\partial n_{1,k}}{\partial t} \right|_{scatt}, \tag{46}$$

$$\frac{J_{\kappa 1,i,k}}{dt} = -i \left(e_{L,k} - e_{2,k} \right) J_{\kappa 1,i,k} - \frac{i h_{i,k,\kappa 1}}{\hbar} \left(n^L_{\kappa 1} - n_{2,k} \right) + \left. \frac{\partial J_{\kappa 1,i,k}}{\partial t} \right|_{scatt}, \tag{47}$$

$$\frac{J_{\kappa 2,i,k}}{dt} = -i \left(e_{1,k} - e_{R,k} \right) J_{\kappa 2,i,k} - \frac{i h_{i,k,\kappa 2}}{\hbar} \left(n_{1,k} - n^R_{\kappa 2} \right) + \left. \frac{\partial J_{\kappa 2,i,k}}{\partial t} \right|_{scatt}, \tag{48}$$

$$n^L_{\kappa 1} = f^L, \tag{49}$$

$$n^R_{\kappa 2} = f^R. \tag{50}$$

$$e_{i,k} = \frac{\varepsilon_{i,k}}{\hbar} - \frac{1}{\hbar}\sum_{k' \neq k} V^{iiii}_{|k'-k|} n_{i,k'} \tag{51}$$

$$\omega_{R,k} = \frac{d_{12}E(z,t)}{\hbar} + \frac{1}{\hbar}\sum_{k' \neq k} V^{iiii}_{|k'-k|} P_{k'} \tag{52}$$

here $e_{i,k}$ is the renormalized transition frequency; $\omega_{R,k}$ is the renormalized Rabi frequency; $e_{R,k} = \varepsilon_{R,k}/\hbar$ and $e_{L,k} = \varepsilon_{L,k}/\hbar$

Equations (49) and (50) reflect approximation of the stationary carrier distribution in bathes. Thus, the kinetic equation is not necessary, and Fermi-Dirac distribution functions can be uses for the approximation. The expressions (51) reflects the renormalization of the transition frequency due to exchange interactions. Also, electron-electron interactions lead to the renormalization of the Rabi frequency represented by Eq. (52). Equations (44)-(46) have the form similar to the semiconductor Bloch equations [Haug (2004)]. Dissimilarities lie in additional terms describing electron transport between the active region and bathes. Additional equations are appeared to provide self-consistent treatment of the electron transport.
As in the previous section, we use the fourth order Runge-Kutta method to solve the problem numericaly [Chow (1999)].

3.3 Band structure, single-particle optical response in quasi-equilibrium

Inclusion of the strain effects in the consideration leads to strong modification of the electron dispersion as well.
Band structures of both interband and intersubband heterostructures are schematically shown in Fig.8. The heterostructures of both kinds have additional subband structure inside the allowed bands. In the interband structures the optical radiation is a result of electron transitions from the conduction subband to the valence subband. As a result, the minimal quantum of the energy is limited by the band gap of the quantum-well material. Curvatures of the bands involved in the transition have very different magnitudes and, what is more important, different senses of curvature. It results in the joint density of states which is stepped one in this case.
Optical transitions in the quantum-cascade heterostructures occur between subbands within an allowed band (see Fig. 8(b)). In contrast to the interband heterostructures, the subband structure is governed by the conduction band offset and width of the qauntum well layer. Minimal transition energy is not limited by the fundamental band gap and can be tailored by a material composition of the quantum well and the thickness of the quantum-well layer. Therefore, quantum-cascade structures are widely used to achieve lasing in THz range. The charge carriers inside the band are characterized by the effective mass The curvature of dispersion curves is almost the same, and their senses of curvature are coincided. It results in the narrow joint density of states, Fig.8(b). Although difference in the curvature of the dispersion curves can be small, it has great influence on the optical characteristics of the quantum-cascade structures. We have examined three cases when subbands with different curvatures are involved in the optical transition. They are shown schematically on Fig.9, where E_{f1} and E_{f2} are quasi-Fermi levels for corresponding subband.
Different relations between effective masses for subbands leads to different absorption spectra. When $m_1 > m_2$ we have $\hbar\omega|_{k=0} > \hbar\omega|_{k\neq 0}$. On the contrary, we have $\hbar\omega|_{k=0} < \hbar\omega|_{k\neq 0}$

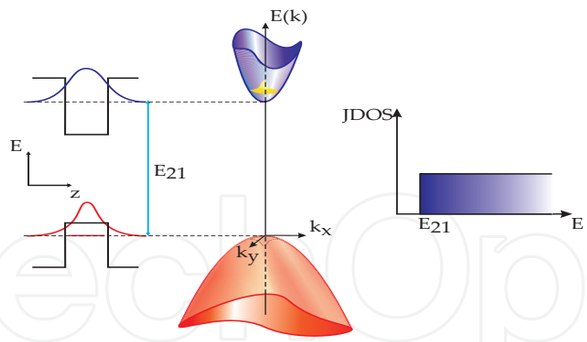

(a)

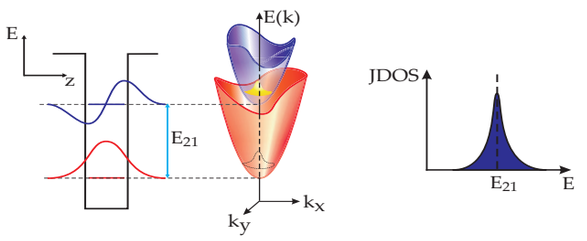

(b)

Fig. 8. Sketches of the band diagrams, band structures and joint DOS for two cases of interband and intersubband transitions.

when $m_1 < m_2$. And, in the case of equal effective masses, one gets $\hbar\omega|_{k=0} = \hbar\omega|_{k\neq 0}$. Fig. 10 contains calculated single-particle absorption spectra. Vertical line indicates the energy of intersubband transition E_{12} at the center of the Brillouin zone without renormalization , i.e. $E_{12} = E_1|_{k=0} - E_2|_{k=0}$. Two important features are observed. Depending on the relation between the effective masses in the subbands, maximum of the absorption get red- or blue-shifted relative to the case of the equal effective masses. The value of the shift is about 20 meV, what is very important in the THz range. Difference of effective masses leads to additional broadening of the absorption spectrum and decreasing of its maximum comparing with the case when effective masses are equal. Thus, the band structure with energy-dependent effective mass affects strongly on optical response of QCS.

3.4 Many-body effects within the Hartree-Fock approximation

In this section, we take quick look at many-body effects in the QCS at the Hartree-Fock level of approximations. At this level of approximations, electron-electron interaction effects are described in the frame of the mean-field approximation when only exchange interactions and Rabi frequency renormalization are taking into account. Fig. 11 contains computed absorption spectra for the quasi-equilibrium regime. Three cases have been considered: single-particle

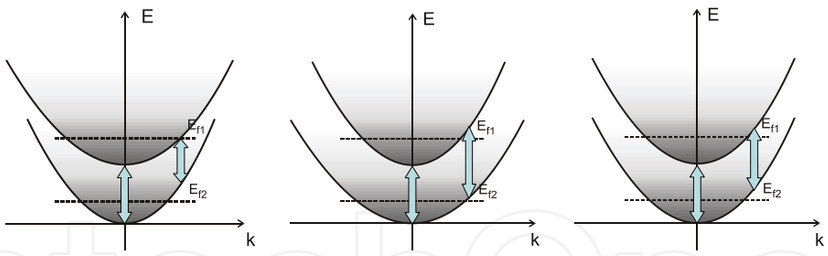

Fig. 9. Sketches of the band structures for various combinations of the effective masses in two subbands involved in radiation transitions: a) $m_1 > m_2$; b) $m_1 < m_2$; c) $m_1 = m_2$.

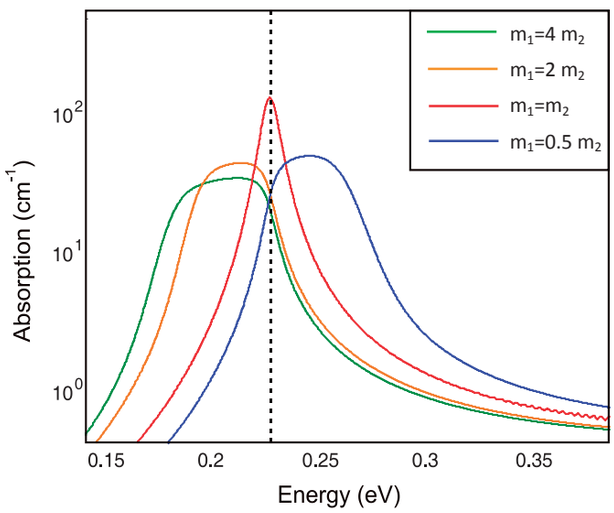

Fig. 10. Single-particle absorption spectra for various combinations of the effective mass in two subbands involved into radiation transitions.

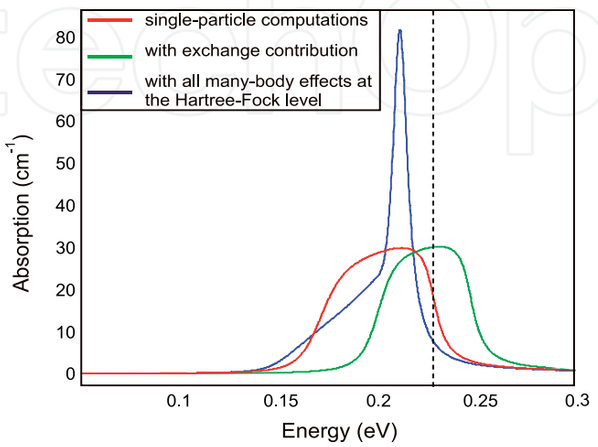

Fig. 11. Many-body effects in the optical absorption spectrum

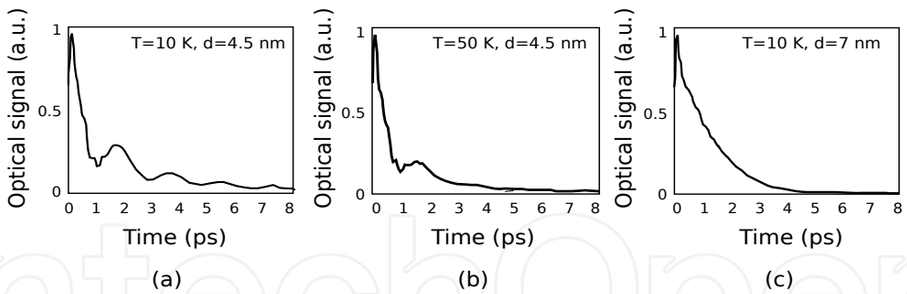

Fig. 12. Optical signals in pump-probe experiments. Adapted from [Weber et al (2009)].

optical response, effect of transition energy renormalization due to the exchange contribution and all many-body effects at the Hartree-Fock level of approximation including Rabi frequency renormalization. All these cases are attended by dephasing treated phenomenologically. Presented results are evidence of high importance of many-body effects which lead to dramatical changes in absorption spectra. In Fig. 11, the dashed line marks energy gap between subbands at the center of Brillouin zone $(k = 0)$.

The exchange energy term causes shifting of the absorption spectra into high energies. Contribution of the exchange energy term leads to decreasing of energy for electrons populating subbands. Energy reduction for each subband is proportional to its electron population. Therefore, transition energy is increased if a lower subband contains more carriers comparing with higher one. In the opposite case, when higher subband is more populated, the transition energy is decreased. Both cases have been reported in papers [Mi (2005)] for the first case and [Pereira (2004)] for the second one). That is the distinguished feature of intersubband transitions. Energy of interband transitions is always decreased if the exchange contribution is taking into account. Energy of intersubband transitions can be shifted in any directions depending on subbands populations.

Hartree-Fock approximation includes the Rabi frequency renormalization represented in the polarization equation (44). Joint action of the exchange contribution and Rabi frequency renormalization on the spectrum are marked by the blue line in Fig. 11. As follows from results, Rabi frequency renormalization (also known as depolarization) leads to the occurrence of a narrow peak in the absorption spectrum. The frequency corresponding to this peak is the frequency of optically excited coherent collective oscillations in the electron plasma. Such plasma colective oscillations are called the intersubband plasmons [Mi (2005)]. Theory of coupled photon and intersubband plasmon was developed in [Pereira (2007)], and this theory gives rise of new quasiparticle titled antipolariton.

3.5 Electron transport effect

The effects of the coherent transport can be observed in pump-probe experiments at the femtosecond and picosecond time intervals. The pump-probe experiment consists in propagation through the investigated media of two optical pulses shifted in time relative each other. First pump pulse is characterized by high intensity, and it excites optically-active media. The second pulse reads changes in the media undergoing optical absorption or gain. More details about pump-probe techniques can be found in [Weber et al (2009)]. Fig. 12 contains results of pump-probe optical experiments reported in [Weber et al (2009)]. The pump pulse have the shape of the Gaussian function.

Each subfigure corresponds to defined parameters which are the temperature and width of the injection barrier in the QCS. Oscillations of the optical response signal at low temperature and barrier's width is caused by coherent electron transport between active region and injector through the injection barrier. The decay of oscillations with increasing of temperature is effect of many-body interactions. Scatterings leads to destroying of the coherence via dephasing. Represented data also reflects the effect of injection barrier width on electron transport. As have been mentioned above, the coherent electron transport is strongly dependent on the interaction between quantum wells defined by parameters of the potential barrier. As far as the width of barrier is increased, the interaction between quantum wells is decreased and, therefore, the frequency of oscillations is decreased.

4. Conclusions

In this chapter, we have considered influence of the electron transport on the optical properties of quantum-cascade structures. The electron transport can be treated as evolution of the electron distribution function in time and space. On the one hand, optical processes are strongly dependent on this function, and, on the other hand, they cause changes of the distribution function due to radiative transitions of charge carriers. Therefore, transport and optical processes are strongly coupled via the electron distribution function. This situation is common for all semiconductor structures. However, the case of QCS has many particularities connected with intersubband transitions and tunneling coupling of the active regions in neighboring cascades. At very short time intervals, electrons coherently pass from one active region to another through injector. Depending on injectors width and structure, carriers can propagate through whole injector without inelastic scatterings. In the oposite case, electron from the active region makes coherent transitions to some energy level in the injector. Thus, it has been shown that the coherent transport influence optical chacteristics at the time interval been of order up to one picosecond. This result is confirmed by experimental data.

Our consideration is based on the density matrix theory. This approach is appropriate for equilibrium case as well as for non-equilibrium one and open quantum systems. We have derived kinetic equations describing dynamics of the electron distribution function, polarization and tunneling microcurrents.

The single-particle band structure influences strongly the shape of optical absorption spectra. Consideration of the position- and energy-dependent effective mass increases acuracy of obtained results.

Many-body effects are relevant for all operational regimes of QCS. They determine the inhomogeneous broadening of spectral characteristics and their peaks position at the energy scale. The temperature dependence of optical characteristics is caused by many-body effects.

It is necessary to provide future investigations of the interference between electron transport and optical processes including in the consideration many-body interactions in injectors and correlations of electrons through several periods.

5. References

Gmachl, C.; Capasso, F.; Sivco, D.L.; Cho, A.Y. (2001) Recent progress in quantum cascade lasers and applications. *Rep. Prog. Phys.*, 64, 11, November 2001, 1533-1601, ISSN

Iotti, R.C.; Rossi, F. (2001) Nature of charge transport in quantum cascade lasers. *Phys. Rev. Lett.*, 87, 14, October 2001, 146603-1-4, ISSN

Weber, C.; Wacker, A.; Knorr A. (2009) Density-matrix theory of the optical dynamics and transport in quantum cascade structures: The role of coherence. *Phys. Rev. B*, 79, 2009, 165322-1-14, ISSN

Optoelectronic devices: advaced simulation and analysis, Piprek J. (Ed.), Springer, ISBN 0-387-22659-1, New York

Femtosecond laser pulses, Rulliere C. (Ed.), Springer, ISBN 0-387-01769-0, New York

Lee, Y.-S. (2009) *Principles of Terahertz Science and Technology*, Springer, ISBN 978-0-387-09539-4, New York

Lee, S.-C.; Wacker, A. (2002) Nonequilibrium GreenâĂŹs function theory for transport and gain properties of quantum cascade structures. *Phys. Rev. B*, 66, 2002, 245314-1-18, ISSN

Vukmirović, N., Jovanović, V.C.; Indjin, D.; Ikonić, Z.; Harrison, I.; Milanović, V. (2005) Optically pumped terahertz laser based on intersubbnad transitions in a GaN/AlGaN double quantum well. *J. Appl. Phys.*, 97, 2005, 103106-1-5, ISSN

Meier, T.; Thomas, P.; Koch, S.W. (2007) *Coherent Semiconductor Optics*, Springer, ISBN 10-3-540-32554-9, Berlin

Haug, H.; Koch, S.W. (2004) *Quantum theory of the optical and electronic properties of semiconductors*, World Scientific Publishing, ISBN 981-238-609-2, Danvers

Vu, Q.T.; Haug, H.; Koch, S.W.; (2006) Relaxation and dephasing quantum kinetics for a quantum dot in a optically excited quantum wells. *Phys. Rev. B*, 73, 2006, 205317-1-8, ISSN

Faist, J., Capasso, F.; Sirtori, C.; Sivco, D.L.; Hutchinson, A.L.; Cho, A.Y. (1995) Vertial transitions quantum cascade laser with Bragg confined excited state. *Appl. Phys. Lett.*, 66, 05, January 1995, 538-540, ISSN

Klymenko, M.V.; Safonov, I.M., Shulika, O.V., Sukhoivanov, I.A. (2008) Ballistic transport in semiconductor superlattices with non-zero in-plane wave vector. *Physica Stat. Solidi B*, 245, 8, June 2008, 1598-1603, ISSN

Chow, W.W.; Koch, S.W. (1999) *Semiconductor lasers: fundamentals*, Springer, ISBN 3-540-66166-1, Berlin

Mi, X.W.; Cao, J.C.; Zhang, C.; Meng, F.B. (2005) Effects of collective excitations on the quantum well intersubband absorption. *J. Appl. Phys.*, 98, 2005, 103530-1-5, ISSN

Pereira, M.F., Lee, S.-C.; Wacker, A. (2004) Controling many-body effects in the midinfrared gain and terahertz absorption of quantum cascade laser structures. *Phys. Rev. B*, 69, 20, 2004, 205310-1-7, ISSN

Pereira, M.F., (2007) Intersubband antipolaritons: microscopic approach. *Phys. Rev. B*, 75, 19, 2007, 195301-1-5, ISSN

Semiconductor Technologies

Edited by Jan Grym

ISBN 978-953-307-080-3
Hard cover, 462 pages
Publisher InTech
Published online 01, April, 2010
Published in print edition April, 2010

Semiconductor technologies continue to evolve and amaze us. New materials, new structures, new manufacturing tools, and new advancements in modelling and simulation form a breeding ground for novel high performance electronic and photonic devices. This book covers all aspects of semiconductor technology concerning materials, technological processes, and devices, including their modelling, design, integration, and manufacturing.

How to reference

In order to correctly reference this scholarly work, feel free to copy and paste the following:

Mykhailo Klymenko, Oleksiy Shulika and Igor Sukhoivanov (2010). Electron transport Effect on Optical Response of Quantum-Cascade Structures, Semiconductor Technologies, Jan Grym (Ed.), ISBN: 978-953-307-080-3, InTech, Available from: http://www.intechopen.com/books/semiconductor-technologies/electron-transport-effect-on-optical-response-of-quantum-cascade-structures

INTECH
open science | open minds

InTech Europe
University Campus STeP Ri
Slavka Krautzeka 83/A
51000 Rijeka, Croatia
Phone: +385 (51) 770 447
Fax: +385 (51) 686 166
www.intechopen.com

InTech China
Unit 405, Office Block, Hotel Equatorial Shanghai
No.65, Yan An Road (West), Shanghai, 200040, China
中国上海市延安西路65号上海国际贵都大饭店办公楼405单元
Phone: +86-21-62489820
Fax: +86-21-62489821

IntechOpen